Experiments in Fluids (2019) 60:135
https://doi.org/10.1007/s00348-019-2776-4

LETTER

# Cross-spectral analysis of PSP images for estimation of surface pressure spectra corrupted by the shot noise

Yuta Ozawa[1] · Taku Nonomura[1,2] · Bertrand Mercier[3] · Thomas Castelain[3] · Christophe Bailly[3] · Keisuke Asai[1]

Received: 9 June 2019 / Revised: 10 July 2019 / Accepted: 12 July 2019


## Abstract

We proposed applying the cross-spectrum analysis to the unsteady pressure-sensitive paint (PSP) images to eliminate the electronic shot noise component from the pressure fluctuation spectrum. The data of surface pressure fluctuation behind a square cylinder which measured by means of the polymer/ceramic PSP with a frequency response of approximately 5 kHz which is sufficiently high for studying the Kármán vortex shedding was used for the validation of this analysis method. The cross spectrum is compared with the auto-spectrum of PSP images and that of the Kulite pressure transducer that corresponds to the reference signal. The cross spectrum can drastically reduce the electronic shot noise component in the pressure fluctuation spectrum. The second peak of vortex shedding which is not observed in the result of auto-spectrum can be observed thanks to the noise reduction. The convergence of calculation is faster as the size of the spatial area for calculating cross spectrum increases.

### Graphic abstract

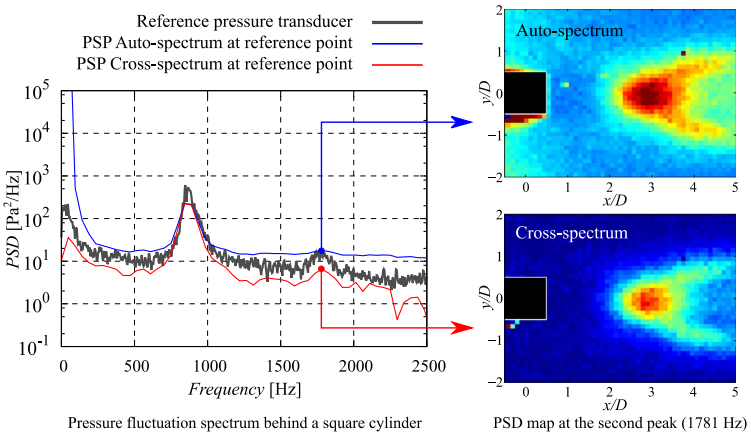


Pressure fluctuation spectrum behind a square cylinder

PSD map at the second peak (1781 Hz)

## 1 Introduction

Surface pressure measurement is an indispensable process in an aerodynamic design of high-speed vehicles. Thus far, pressure transducers and pressure taps on the model surface has often been used for the surface pressure measurement. Limitations of this measurement technique are twofold. First, a detailed mapping of a given model may require a large amount of sensors together with an acquisition system with a large amount of input channels. Second, integration of these sensors in small-scale

✉ Yuta Ozawa
ozawa.yuta@aero.mech.tohoku.ac.jp

[1] Department of Aerospace Engineering, Graduate School of Engineering, Tohoku University, 6-6-01 Aramaki Aza Aoba, Aoba-ku, Sendai, Miyagi 980-8579, Japan

[2] Presto, JST, Sendai, Miyagi 980-8579, Japan

[3] Université de Lyon, École Centrale de Lyon et LMFA UMR CNRS 5509, 69134 Ecully, France

Published online: 29 July 2019

or complex-shape models can be a problem. Therefore, a non-intrusive technique based on pressure-sensitive paint (PSP), using a pressure-sensitive luminescent dye has been developed to allow for measuring the surface pressure distribution on models (Liu and Sullivan 2005; Bell et al. 2001; Gregory et al. 2001). In this recent technique, a model painted with PSP is exposed to excitation light and a recording of the dye luminescence is performed. The luminescence is linked with the local pressure as expressed by the Stern–Volmer equation, as shown in the following equation:

$$\frac{I_{\mathrm{ref}}}{I} = A(T) + B(T)\frac{P}{P_{\mathrm{ref}}}, \tag{1}$$

where $I$ is the luminescent intensity and $P$ is the pressure and the subscript ref stands for reference conditions at which $P$ and $I$ are known. $A(T)$ and $B(T)$ are the Stern–Volmer coefficients which depends on temperature. The surface pressure can be measured by capturing this luminescence using a CCD or CMOS camera to obtain a two-dimensional surface pressure distribution with high spatial resolution.

The PSP technique has been applied to the unsteady phenomenon in low-speed flow for the development of automobile or railway industries. There are two serious issues when measuring unsteady surface pressure using PSP at low-speed flow conditions. The first issue is the time response of PSP. The usual order of magnitude of the time constant for classical PSP is several hundred milliseconds to several seconds, which may be too large to capture unsteady pressure fluctuations related to the studied flow. However, the time response of PSP is improved by polymer–ceramic PSP (Kitashima et al. 2014; Sugioka et al. 2018), and measurements up to several kHz are achieved. The second issue is the low signal-to-noise ratio (SNR) of PSP measurement due to the low dynamic pressure in a wind tunnel. At low-speed conditions, intensity variations of PSP are less than 1% which is typically smaller than the shot noise of a camera. Moreover, for unsteady measurements, the acquired images become much darker, because the exposure time of a camera becomes small. Consequently, unsteady PSP measurements in the low-speed wind tunnels become significantly difficult, because the SNR decreases for estimation of pressure fluctuation as well as for time averaged pressure measurements as the images are darker. Several methods were developed to improve SNR of PSP. Table 1 summarizes the methods that can improve SNR of PSP. A simple measurement technique for solving this problem is a phase-lock measurement which accumulates the synchronized snapshots at the same phase of periodic phenomena based on a reference signal. However, this method can only be applied to periodic flows. On the other hand, various data post-processing methods have been proposed in the literature. Yorita et al. (2010) conducted conditional averaging. They classified time-series PSP images acquired by a high-speed camera into several phases defined by the reference pressure data and averaged them to improve the SNR. Nakakita (2011) applied fast-Fourier transform (FFT) to PSP images. He also showed that the subtraction of power spectral density

**Table 1** Methods to improve SNR of the unsteady PSP measurements

| Approach | Measurement | Signal, data processing | | | | | |
|---|---|---|---|---|---|---|---|
| Name | Phase-lock measurement | Conditional average | Discrete Fourier transform method | | | SVD | EKFDMD |
| | | | FFT | COP | Cross-spectrum (current work) | | |
| Reference signal | Necessary | Necessary[1] | Unnecessary | Necessary[1] | Unnecessary | Unnecessary | Unnecessary |
| Advantage | A), C) | A), C) | B), D) | B)[2], C), D) | B), D) | B), D) | B), D) |
| Disadvantage | E) | E) | F) | E)[2] | G), H) | I) | I) |

A) Possible to increase averaging number

B) Possible to analyze phenomenon in various frequencies

C) Possible to restore a signal below the shot noise

D) Including a phase information

E) Impossible to analyze phenomenon in out of a target frequency

F) Impossible to restore a signal below the shot noise

G) Excluding a phase information

H) Need large amount of data

I) Need to select parameters manually, ex) Number of modes. Noise level

[1]Possible to select another pixel instead of the reference signal

[2]Limited to phenomenon that correlate with the reference signal

(PSD) from the wind-on image to the wind-off image is an effective way to reduce the noise component (Nakakita 2013). Noda et al. (2018) used the coherent output power (COP), which involves the cross correlation between a PSP data and a reference signal, and successfully measured the pressure fluctuations associated with tonal trailing edge noise for a two-dimensional NACA 0012. Pastuhoff et al. (2013) applied singular value decomposition (SVD) to improve the SNR of PSP images with a manual selection of some analytical parameters required by the method. In addition, there are a lot of attempts to apply the modal analysis such as SVD or DMD for unsteady PSP images (Gordeyev et al. 2013; Ali et al. 2016; Penget al. 2016; Roozeboom et al. 2016; Crafton et al. 2017). Nonomura et al. proposed further noise reduction using extended Kalman filter dynamic mode decomposition (EKFDMD) after SVD processing (Nonomura et al. 2018, 2019). These previous works successfully reduced the noise component of PSP images. However, the advantages and disadvantages of these methods are different from each other, as shown in Table 1. From the viewpoint of the simplification of the measurement system, and ease of signal processing, the method chosen for SNR enhancement should ideally not require any reference signal or manual parameters.

In this study, we propose the application of a cross-spectral analysis to a sequence of PSP images to reduce the contribution of the electronic shot noise component in the pressure spectra evaluated from the PSP images. The proposed method is an adaptation of cross-spectral analysis for the Rayleigh-scattering-based density-measurement technique which can drastically reduce the electronic shot noise component when estimating PSD (Panda and Seasholtz 2002; Mercier et al. 2017; Mercier and Castelain 2019). This approach is based on the fact that the intensity variation due to any coherent signal is statistically independent from that due to shot noise. The proposed method is applied to the characterization of surface pressure fluctuations behind a surface-mounted square cylinder. The effectiveness of the proposed method is evaluated by comparing these results to reference measurements from a Kulite pressure transducer.

## 2 Experimental apparatus

### 2.1 Unsteady pressure-sensitive paint (PSP)

The pressure-sensitive paint is a pressure sensor utilizing photochemical reaction that consists of luminescent molecules (luminophore) and binder (mainly polymer). The luminophore becomes luminescent when being illuminated by excitation light with the appropriate wavelength. Since the intensity of emitted light from luminophore depends on the partial pressure of the oxygen, the air pressure over the PSP coating can be calculated from its measured luminescent intensity. A fast-response polymer/ceramic PSP is used in this study (Kitashima et al. 2014; Sugioka et al. 2018; Scroggin et al. 1999; Sakaue et al. 2011; Pandey and Gregory 2015). The pressure sensitivity of PSP measured by static calibration was 0.67%/kPa. Moreover, frequency response of approximately 5000 Hz was guaranteed from the result of frequency response measurements using an acoustic resonance tube (Sugimoto et al. 2012). In the following, the frequency analysis will thus be restricted to a maximum of 5 kHz. This value is greater than two times the shedding frequency in the cylinder wake.

### 2.2 Experimental model and measurement system

We referred the experimental data of the surface pressure fluctuation behind a square cylinder for the validation of this analysis method (Hiura et al. 2017; Sugioka et al. 2019). The experiment was conducted in the Tohoku-University basic aerodynamic research wind tunnel (T-BART) of cross section 300×300 mm. It consisted in the measurement of pressure field over a ground flat plate in the vicinity of a square cylinder flush-mounted on a plate. Various cylinder side lengths $D$ have been considered from $D=3.25$ mm to $D=40$ mm. The test conditions, including the value of the Reynolds number based on the cylinder side length and the expected frequency of Kármán vortex shedding, are reported in Table 2. A CAD view and a picture of the model with the ground plate are shown in Fig. 1a, b, respectively. During the experiment, the model is fixed at the center of a turntable to which PSP measurement can be applied. The diameter of the turntable and the distance from the front edge of the ground plate to the center of the turntable are 250 mm.

The measurement system is shown in Fig. 1c, d. Unsteady PSP measurements were synchronized with the recording of the Kulite pressure transducer (XCL-152-5SG) flush-mounted on the ground plate. The distance between the cylinder center and the pressure tap connected to the Kulite sensor is 1.8$D$ in the axial direction and 0.5$D$ in the transverse direction, as depicted in Fig. 1e. The Kulite sensor frequency response is 150 kHz, which is significantly higher than that of the unsteady PSP. The perpendicular and transverse acceleration sensitivities of the Kulite sensor are $1.5\times10^{-3}$% FS/g and $2.2\times10^{-4}$% FS/g, respectively. For the unsteady pressure measurement system, the signal was amplified by an amplifier (SA-570ST, TEAC), and recorded with the data logger (WE 7000, Yokogawa) after applying an analog filter (3625,

**Table 2** Test conditions

| $D$ [mm] | 3.25 | 6.5 | 13 | 40 |
|---|---|---|---|---|
| Reynolds number $Re_D$ [$\times10^4$] | 1.1 | 2.1 | 4.3 | 13 |
| Peak spectrum frequency $f$ [Hz] | 2000 | 1000 | 500 | 150 |

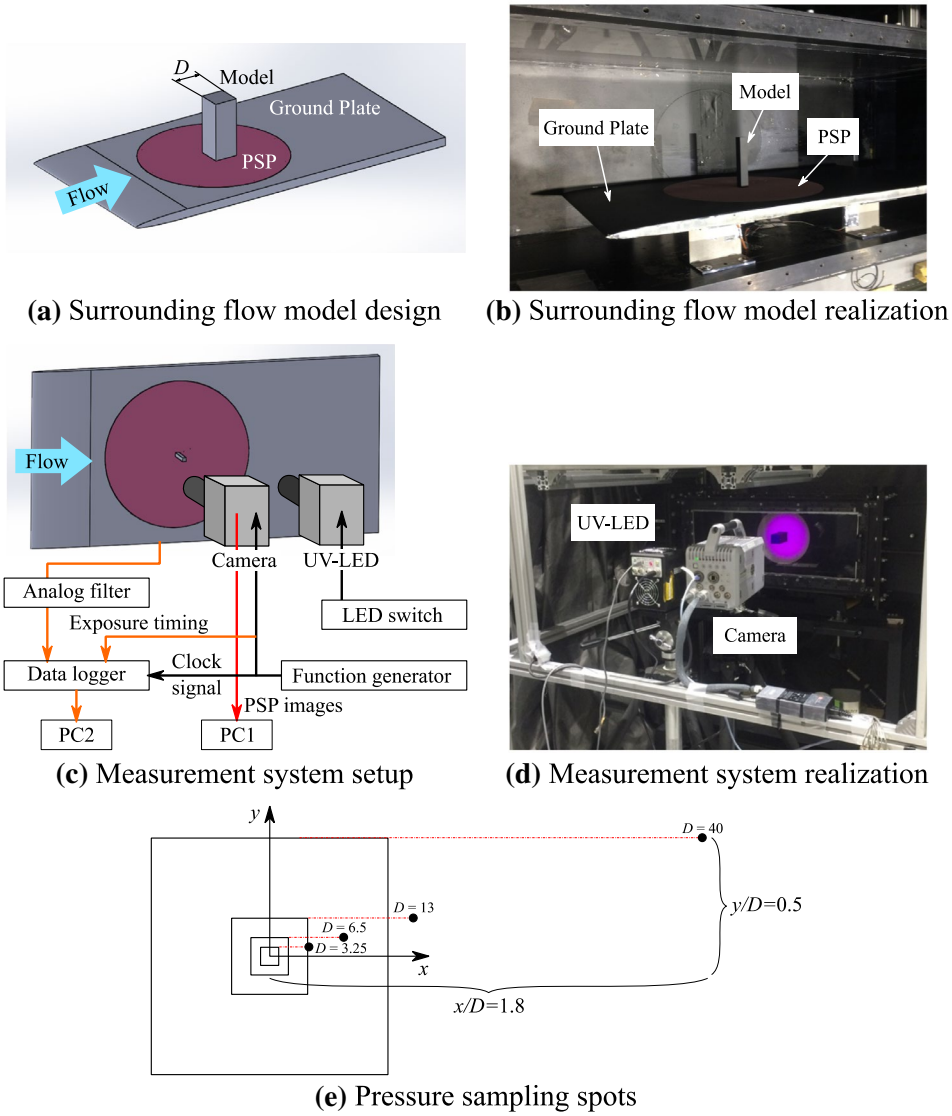


**(a)** Surrounding flow model design

**(b)** Surrounding flow model realization

**(c)** Measurement system setup

**(d)** Measurement system realization

**(e)** Pressure sampling spots

**Fig. 1** Experimental model and system of the surrounding flow measurement

NF). For the PSP measurement system, a UV-LED (IL-106, Hardsoft) was used with a condenser lens (HSO-PL-180-UV, HArdsoft) as an excitation light source for the PSP. A high-speed camera (SA-X2, Photron) was used as a light emission detector. The camera was fitted with a 50 mm focal length lens (Nikkor 50 mm f 1.2, Nikon) and a 650 ± 20 nm bandpass filter (PBO 650-040, Asahi Spectra). The detailed measurement conditions are presented in Table 3. The references describe the more details of the measurement condition (Hiura et al. 2017; Sugioka et al. 2019).

## 2.3 Data analysis

The overall flow of basic PSP data process is shown in Fig. 2. The pressure distribution time series are calculated using the Stern–Volmer equation, as shown in Eq. 1. In this study, the image obtained by averaging the wind-on images and performed the dark subtraction is used as the reference image $I_{ref}$. This method allows reducing the influence of the change in the luminescent intensity due to the temperature change or photo-degradation of the luminophore, but only gives access to the pressure fluctuations. Subsequently, PSD of the pressure fluctuations are calculated based on the time-series pressure distribution using the FFT, as done by Nakakita (2011, 2013). The auto-spectra calculated using the FFT were ensemble averaged.

## 2.4 Proposed method using cross spectrum

In the previous studies, Panda and Seasholtz (2002) used cross spectra to reduce the shot noise of density fluctuations spectra obtained by Rayleigh-scattering measurement. They measured the density fluctuations in the plumes of a fully expanded jet using two photomultipliers which both probe

**Table 3** Measurement conditions and FFT parameters in the experiment

| $D$ [mm] | 3.25 | 6.5 | 13 | 40 |
|---|---|---|---|---|
| PSP images | | | | |
| Acquisition parameters | | | | |
| Frame rate [fps] | 24,000 | 12,000 | 6000 | 1800 |
| Exposure time [s] | 1/25724 | 1/12419 | 1/6102 | 1/3703 |
| Resolution [px] | 640×576 | 640×640 | 1024×704 | 1024×888 |
| Number of images | 62,124 | 55,911 | 31,767 | 25,814 |
| FFT parameters | | | | |
| FFT data length | 256 | 256 | 256 | 256 |
| Number of averaging | 480 | 430 | 244 | 190 |
| Frequency resolution | 94 | 47 | 23 | 7.0 |
| Pressure transducer | | | | |
| Acquisition parameters | | | | |
| Sampling rate [Hz] | 72,000 | 72,000 | 72,000 | 72,000 |
| Cutoff frequency [Hz] (low-pass) | 36,000 | 36,000 | 36,000 | 36,000 |
| FFT parameters | | | | |
| FFT data length | 16,384 | 16,384 | 16,384 | 16,384 |
| Number of averaging | 20 | 20 | 20 | 20 |
| Frequency resolution | 4.4 | 4.4 | 4.4 | 4.4 |

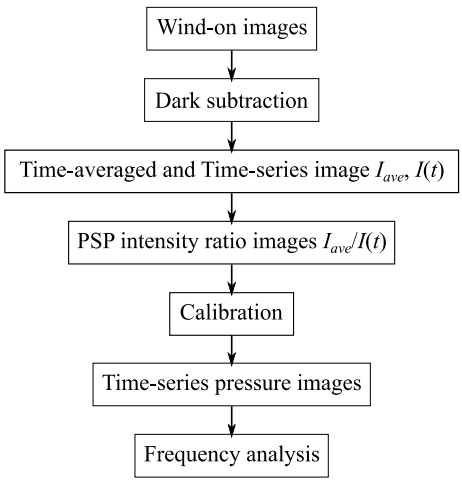


**Fig. 2** Flow chart of the PSP data process

the same volume. Computing the cross spectrum between two photomultiplier signals was shown to drastically reduce the electronic shot noise contribution. Mercier et al. (2017) proposed an adaptation of this method which requires only one photomultiplier. They made two different time-series signals from the single photomultiplier measurement by alternately dividing the original signal, and proved that the cross spectrum between these two signals provides a good estimate of the density fluctuation spectrum with a limited residue of shot noise. From these previous works, it has been shown that the signal processing using cross spectrum is effective to reduce the electronic shot noise contribution because of its statistical properties.

In the case of unsteady PSP images at the low wind tunnel tests, the SNR is significantly low due to the low dynamic pressure. Therefore, the pressure fluctuation spectrum will be significantly affected by the electronic shot noise contribution. Fortunately, PSP images acquired by a high-speed camera have a high spatial resolution; thus, the nearby several pixels are considered to represent the same pressure fluctuation. Therefore, we can propose another adaptation of the above methods for estimating the PSD of the unsteady PSP images.

We assume that the nearby several pixels on the PSP images represent the same pressure fluctuations. Here, the intensity signals of two nearby pixels are represented by $I_1$ and $I_2$. These intensity signals are divided into $m$ segments of a length determined from the frequency resolution $\Delta f$:

$$I_1^j, I_2^j \quad (j = 1, 2, 3, \ldots, m) \tag{2}$$

and that can overlap. The Fourier coefficients of each segment $Y_{I1}^j$ and $Y_{I2}{}^j$ are decomposed into the pressure fluctuation $P^j$ and the shot noise contribution $W^j$

$$Y_{I1}^j(f) = P_{I1}^j + W_{I1}^j \tag{3}$$

$$Y_{I2}^j(f) = P_{I2}^j + W_{I2}^j, \tag{4}$$

where we would like to remove the shot noise contribution from the PSD, and only retain the pressure fluctuations. To eliminate the shot noise contribution, the cross spectrum

between these two signals $C_{I1I2}$ is calculated by averaging the Fourier coefficient of the $m$ segments:

$$C_{I1I2}(f) = \frac{2}{m}\sum_{j=1}^{m} Y^{j}_{I1}(f)Y^{j*}_{I2}(f). \tag{5}$$

In this equation, * denotes the complex conjugate. This cross spectrum can be recast into the following expression:

$$\begin{aligned} C_{I1I2}(f) = \frac{2}{m}\sum_{j=1}^{m} & W^{j}_{I1}(f)P^{j*}_{I2}(f) + P^{j}_{I1}(f)W^{j*}_{I2}(f) \\ & + W^{j}_{I1}(f)W^{j*}_{I2}(f) + P^{j}_{I1}(f)P^{j*}_{I2}(f). \end{aligned} \tag{6}$$

The number of segments $m$ assumed to be sufficiently large. Thus, the products of pressure fluctuation $P_j$ and the shot noise contribution $W_j$ approaches zero, because these two contributions are statistically independent. The products of shot noise contribution at each pixels $W_{I1}{}^{j}$ and $W_{I2}{}^{j}$ also tends to zero, because the shot noise at each pixel is statistically independent. Therefore, the cross spectrum of two pixels can be approximated by the following relationship:

$$C_{I1I2}(f) \approx \frac{2}{m}\sum_{j=1}^{m} P^{j}_{I1}(f)P^{j*}_{I2}(f). \tag{7}$$

Finally, the PSD of the pressure fluctuations can be estimated to be the absolute value or the real part of Eq. (5). This is because the imaginary part should become zero when the shot noise contribution sufficiently decreases (for instance, as $m$ is sufficiently large), because the phase difference between the pressure signals of the two nearby pixels is zero. In the present study, we adopt the absolute value of Eq. (5) to avoid the negative estimated power. Note that the absolute value of Eq. (5) may slightly increase PSD level when it is not converged, because the imaginary part of the Eq. (5) which is statistically a residual component have a trend to increase the PSD level theoretically, while it avoids the estimation of the negative power as mentioned before. This implies that the estimation has the trend of the overestimation when it is not converged.

Figure 3 shows a schematic that describes the analysis methods for estimating pressure fluctuations. The left image shows the raw PSP image colored with the intensity of pixels. In this image, the black solid box on the left side represents the square cylinder. To calculate the cross spectrum of pressure fluctuations, we divided original images into spatial areas which consist of $N\times N$ pixels and assumed that the pressure fluctuations are identical within the $N\times N$ pixels. This dividing corresponds to reducing spatial resolution of the original image to $1/N\times 1/N$. An example of calculation when $N$ equal to 4 is also displayed in Fig. 3. Cross spectrum of pressure fluctuations can be calculated from all combination of two pixels in the spatial area. The number of combinations in the spatial area is determined from the combination formula:

$${}_{N\times N}C_2 = \frac{(N\times N)!}{2!(N\times N-2)!}. \tag{8}$$

Therefore, the pressure fluctuation spectrum in the spatial area is calculated as the average of $m\times {}_{N\times N}C_2$ cross spectra.

In this study, we processed the unsteady PSP images using the fast Fourier transformation (FFT). The FFT parameters are shown in Table 3. In all the cases, FFT are calculated with 50% overlapping samples for the temporal direction. Figure 4 shows the pressure fluctuation spectra of $D=6.5$ mm calculated by the proposed method using various FFT parameters. The spectra are calculated with a size of the spatial areaof $N=4$. The pressure fluctuation spectra become smoother with increasing the number of averaging (decreasing the frequency resolution), because the shot noise level decreases with the square root of the number of ensemble averages (Mercier and Castelain 2019). In this paper, the frequency resolution of the FFT is set to be relatively

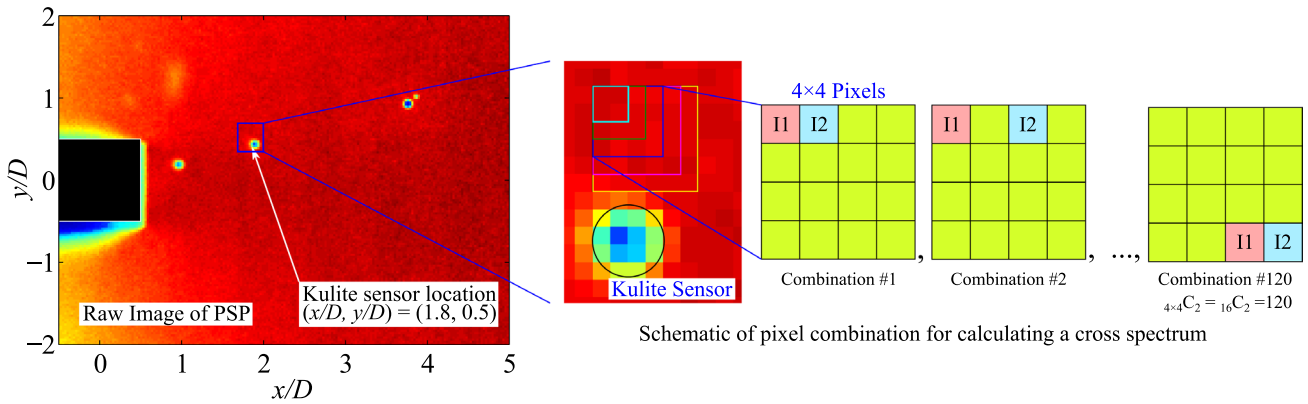


**Fig. 3** Schematic of the analysis using cross spectrum

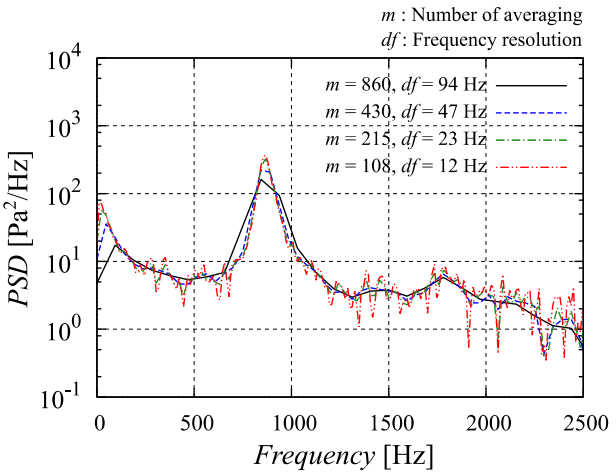


**Fig. 4** Effect of FFT parameters on the cross spectra calculated by the proposed method

low, because the reduction of the shot noise components requires a large number of ensemble averages $m$. We also calculated auto-spectrum of $N \times N$ averaged pixels using the same parameters to compare the results.

## 3 Results and discussion

### 3.1 Comparison between auto-spectrum and cross-spectrum

A comparison of the pressure fluctuation spectrum estimated from PSP measurements to that derived from pressure sensor measurements is given in Fig. 5. The process is applied to the four cylinders tested here. The results are obtained by applying the data processing method described in Sect. 2.4 with $N=4$ are compared to the auto-spectrum evaluation on the same area. All the pressure fluctuation spectra clearly show the first peak at the frequency of the Kármán vortex shedding. For the reference spectrum acquired by the Kulite pressure transducer, the small second peak appears in the case $D=6.5$ mm. However, for the auto-spectra calculated from unsteady PSP images, the second peak in the case of $D=6.5$ mm and 13 mm cannot be observed because of noise floor of shot noise. On the other hand, the cross spectrum calculated by the proposed method can capture the low amplitude second peak in these cases. The shot noise of PSP images is well eliminated in those cases. For $D=3.25$ mm,

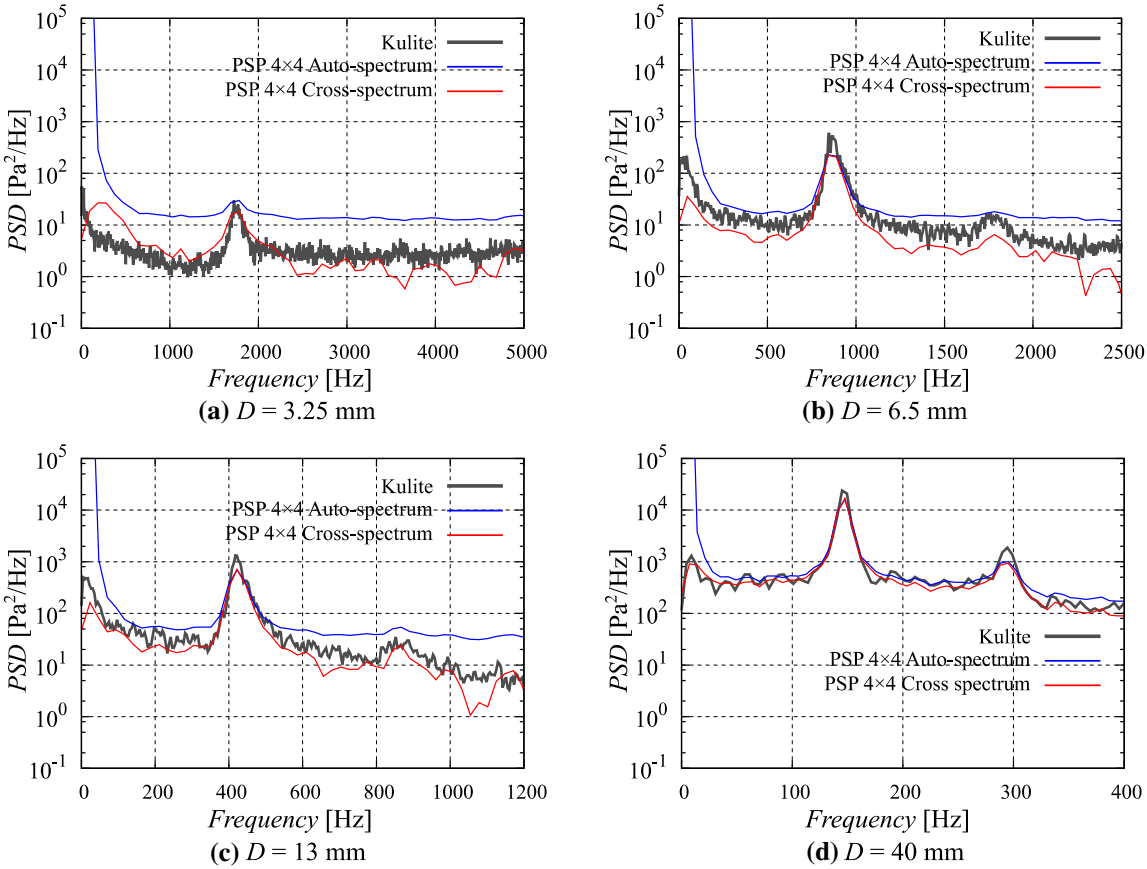


**Fig. 5** Comparison of pressure fluctuations spectrum between reference spectrum acquired by the Kulite pressure transducer and that of unsteady PSP

the second peak cannot be observed, because the dynamic pressure is too low.

In all cases, the noise floor level in the pressure fluctuation spectra calculated from cross spectrum drastically decreases in comparison with that of the auto-spectrum except the case of $D=40$ mm. In the case of $D=40$ mm, even in the auto-spectrum, the pressure fluctuation spectrum shows good agreement with that of the reference signal, because the pressure fluctuation is much larger than those of the cases of the diameter less than 13 mm. Therefore, the SNR is sufficiently high compared with the shot noise in the case of $D=40$ mm. In the case of the diameter less than 13 mm, the noise floor calculated using cross spectrum is less than that of Kulite pressure transducer. In the case of $D=13$ mm, the cross spectrum depicts a sharp drop around the frequency of 1100 Hz. This seems to be due to the insufficient convergence of cross-spectrum calculation. The convergence of the cross-spectrum calculation is investigated in the next section.

The distribution of pressure fluctuations estimated from the PSP images will be discussed only in the case $D=6.5$ mm for which the relevancy of the cross-spectrum method appears clearly as shown in Fig. 5b with a decrease by nearly one order of magnitude of the noise floor. Figure 6 shows the comparison of PSD distribution at the first and second peak frequencies. At the frequency of first peak, the PSD distributions calculated by auto-spectrum and cross spectrum do not significantly change. This is because the pressure fluctuation at the frequency of first peak is sufficiently large in comparison with the electronic shot noise component. Nevertheless, a large difference appears in the PSD distributions at the frequency of second peak, while the distribution is the same in the region of large level of fluctuations. In the PSD distribution calculated from the auto-spectrum, the power all over the image is relatively high in comparison with that calculated from the cross spectrum. As shown in Fig. 5, the pressure fluctuation at the second peak is significantly smaller than that at first peak. Therefore, the result of the proposed method using cross spectrum is much more effective for the reduction of the electronic shot noise component.

### 3.2 Effects of a size of the spatial area

As mentioned in Sect. 2.4, we can increase the number of spatial averaging $N\times N$ to faster converge the calculation of the cross spectrum. We investigated the effect of the number $N$

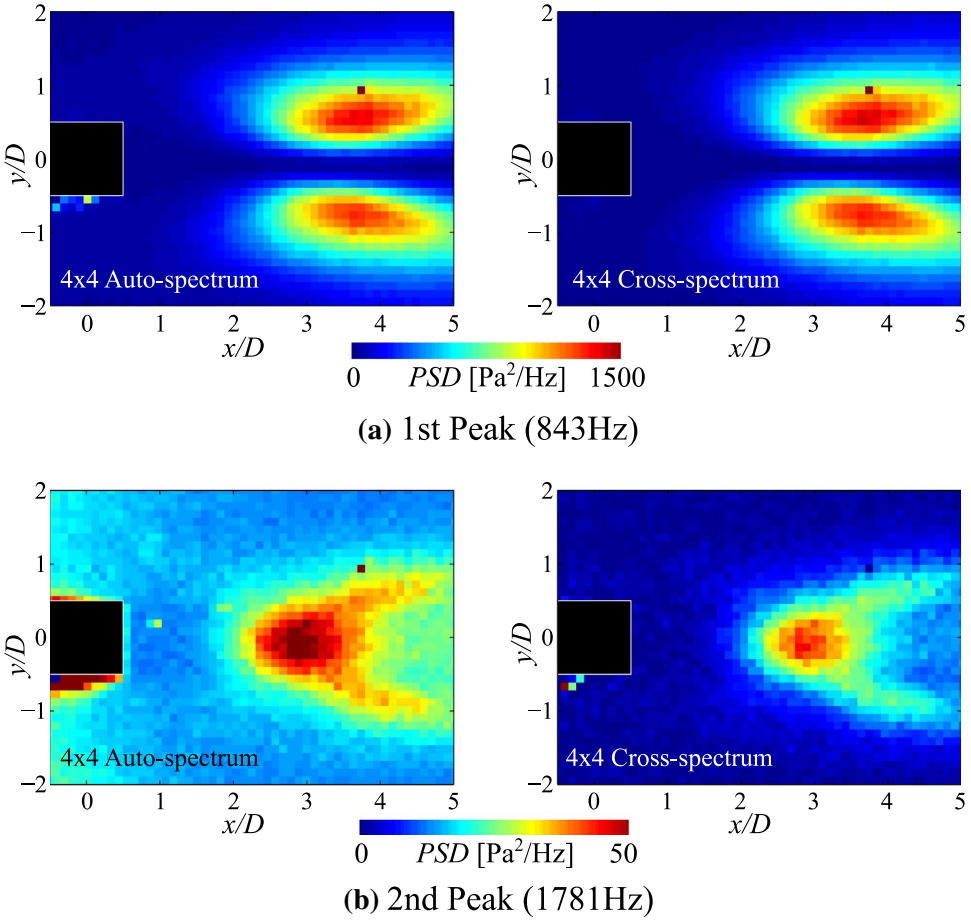


**Fig. 6** Comparison of the PSD distributions between the auto-spectrum and the cross spectrum at the first and second peak frequencies. The black solid box represents the cross-sectional square cylinder

for the diameter 6.5 mm case. Figure 7 shows the effects of the size of the spatial area on the pressure fluctuation spectrum at the reference point for $N$ ranging from 2 to 20. Table 4 shows the number of averaging for calculating the pressure fluctuation spectrum. The number of temporal averaging was determined from the parameters for FFT, as shown in Table 3, and the number of spatial averaging was determined using Eq. (8). Therefore, the total number of averaging can be calculated by multiplying them. In this study, the number of temporal averaging was set to 430, so that the frequency resolution of the cross spectra is constant and is equal to 47 Hz. For all cross spectra, Fig. 7 shows that the first peak frequency is 843 Hz and the shot noise contribution drastically decreases. In the case of $N=2$, the cross spectrum has the large variation in the noise floor of the entire frequency range. Moreover, most of the large variation on the spectrum disappears in the case of $N=4$, while the spectrum has a minus peak at the frequency of 2.3 kHz. This large variation of the spectrum disappears in the case of $N>4$ and the spectra become smoother. The large variation of the spectrum seems to be due to the insufficient convergence of the cross-spectrum calculation, because these non-physical spectra disappear with increasing the total averaging number. The convergence of the calculation seems to be faster in the low-frequency region. These characteristics of the cross spectrum imply that the number $N$ should be larger for studying high-frequency phenomena, while the spatial area determined by $N$ should measure the same pressure fluctuation. Note that the convergence of the calculation may also be faster with increasing the number of temporal averaging, while the frequency resolution decreases. The second peak of the spectrum is smoothed in the case of $N>10$ in comparison with the case of $N=4$. This is because the assumption that the $N\times N$ pixels in the spatial area measure the same pressure fluctuations is not valid anymore. In this study, the spatial area determined by the number $N$ is inside the region, where the second peak is dominant when the $N$ is less than 4. On the other hand, when the number $N$ increases, the spatial area does not only include the region, where the second peak is dominant, but also the region, where the second peak is weak. Therefore, the second peak vanishes with an increase in the number $N$. The convergence of calculation is a tradeoff relationship with the size of the spatial area. Practically, the size of the spatial area should be determined considering the assumption that the nearby pixels have the same pressure fluctuation. This will be based on the resolution of the image sensor and the optical setup of a camera.

### 3.3 Effects of the temporal averaging number

The convergence of the calculation is also affected by the number of temporal averaging $m$. We investigated the effects of the averaging number $m$ for the diameter 6.5 mm case. Figure 8 shows the effects of the temporal averaging number on the pressure fluctuation spectrum at the reference point. The spectra shown in Fig. 8 are calculated with the spatial area of $N=4$. The total number of averaging is shown in Table 5, and the frequency resolution of the cross spectra is constant and equal to 47 Hz, as shown in Table 3. The pressure fluctuation spectra basically become smoother with increasing the number of temporal averaging. Thus, the convergence of the calculation strongly depends not only on the spatial averaging but also on the temporal averaging. For sufficient convergence without losing the spatial resolution, the number of temporal averaging should increase and longer data lengths are required.

## 4 Conclusion

In this study, we performed a cross-spectral analysis on unsteady PSP images. The surface pressure fluctuations behind a square cylinder were acquired by means of a high-speed camera and polymer/ceramic PSP of which frequency response is approximately 5000 Hz. We applied the proposed method to this unsteady PSP images and

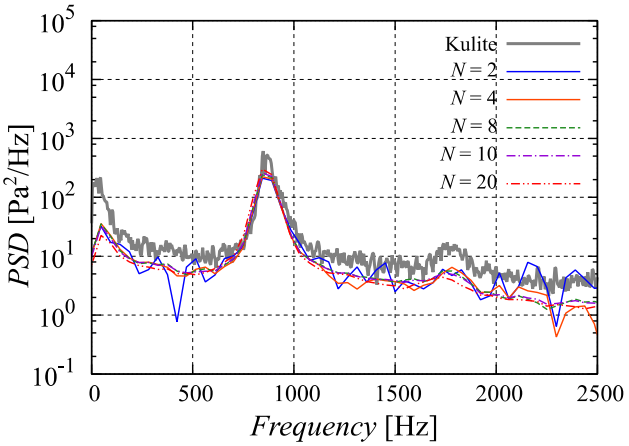


**Fig. 7** Effects of the size of the spatial averaging area on the pressure fluctuation spectrum

**Table 4** Number of averaging for calculating the spectrum

| $N$ | 2 | 4 | 8 | 10 | 20 |
|---|---|---|---|---|---|
| Number of temporal averaging | 430 | 430 | 430 | 430 | 430 |
| Number of spatial averaging | 6 | 120 | 2016 | 4950 | 79,800 |
| Total number of averaging | 2580 | 51,600 | 8,66,880 | 2,128,500 | 34,314,000 |

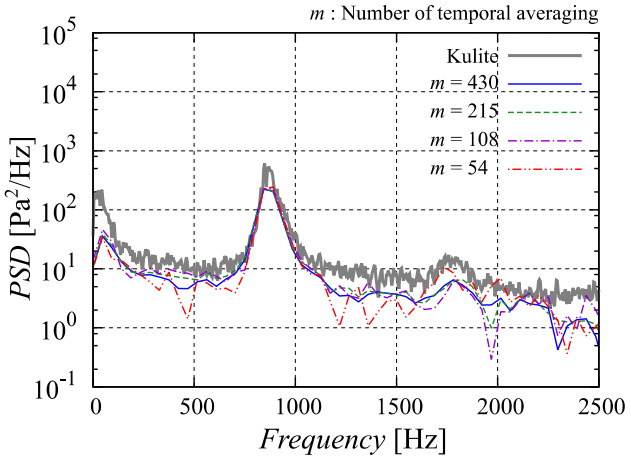


**Fig. 8** Effects of the number of temporal averaging on the pressure fluctuation spectrum

**Table 5** Number of averaging for calculating the spectrum

| | | | | |
|---|---|---|---|---|
| Number of temporal averaging, $m$ | 54 | 108 | 215 | 430 |
| Number of spatial averaging ($N=4$) | 120 | 120 | 120 | 120 |
| Total number of averaging | 6480 | 12,960 | 25,800 | 51,600 |

compared it with the results from a conventional auto-spectral analysis.

The electronic shot noise component in the pressure fluctuations spectra is found to be drastically reduced using the cross-spectrum method. The second peak of the vortex shedding which is not observed in the result of auto-spectrum can be observed thanks to the noise reduction of the proposed method. The convergence rate of the calculations increases as the size of the spatial area and the number of temporal averaging for the cross-spectrum calculation increases. Note that the size of the spatial area should be determined considering the assumption that the nearby pixels measure the same pressure fluctuation.

**Acknowledgements** This study was supported by JST Presto Grant No. JPMJPR1678.

## References

Ali M, Pandey A, Gregory J (2016) Dynamic mode decomposition of fast pressure sensitive paint data. Sensors 16(6):862

Bell JH, Schairer ET, Lawrence A, Hand LA, Mehta RD (2001) Surface pressure measurements using luminescent coatings. Annu Rev Fluid Mech 33:155–206

Crafton JW, Gregory JW, Sellers ME, Ruyten W (2017) Data processing tools for dynamic pressure-sensitive paint. In: 55th AIAA Aerospace Sciences Meeting

Gordeyev S, De Lucca N, Jumper EJ, Hird K, Juliano TJ, Gregory J, Thordahl J, Wittich DJ (2013) The comparison of unsteady pressure field over flat-and conformal-window turretsusing pressure sensitive paint. In:44th AIAA Plasmadynamics and Lasers Conference

Gregory JW, Sakaue H, Sullivan JP, Raghu S (2001). Characterization ofminiature fluidic oscillator flowfields using porous pressure sensitive paint. In: Proceedings ASME Fluids Engineering Division Summer Meeting, FEDSM2001-18058

Hiura K, Sugioka Y, Matsui A, Morita K, Nonomura T, Asai K (2017) Evaluation of accuracy and applicable limit of pressure-sensitive paint for unsteady phenomena at various frequencies in low speed flow. Asia Pacif Int Symp Aerosp Technol 2017:H8-5

Kitashima S, Numata D, Asai K (2014) Characterization of pressure-sensitive paint containing ceramic particles. In: 16th International Symposium on Flow Visualization, ISFV16-1286

Liu T, Sullivan JP (2005) Pressure and temperature sensitive paints. Springer-Verlag, Berlin

Mercier B, Castelain T (2019) Dynamic analysis of a Rayleigh scattering setup using synthetic light signals from a modulated LED. Rev Sci Instrum 90:063109. https://doi.org/10.1063/1.5112802

Mercier B, Castelain T, Jondeau E, Bailly C (2017) Density fluctuations measurement by rayleigh scattering using a single photomultiplier. AIAA J 56(4):1310–1316

Nakakita K (2011) Unsteady pressure measurement on NACA0012 model using global low-speed unsteady PSP technique. In: 41st AIAA Fluid Dynamics Conference and Exhibit, AIAA2011-3901

Nakakita K (2013) Detection of phase and coherence of unsteady pressure field using unsteady PSP measurement. In: AIAA ground testing conference fluid dynamics and co-located conferences, AIAA2013-3124

Noda T, Nakakita K, Wakahara M, Kameda M (2018) Detection of small-amplitude periodic surface pressure fluctuation by pressure-sensitive paint measurements using frequency-domain methods. Exp Fluids 59(6):94

Nonomura T, Shibata H, Takaki R (2018) Dynamic mode decomposition using a Kalman filter for parameter estimation. AIP Adv 8(10):105106

Nonomura T, Shibata H, Takaki R (2019) Extended-Kalman-filter-based dynamic mode decomposition for simultaneous system identification and denoising. PLoS One 14(2):e0209836

Panda J, Seasholtz RG (2002) Experimental investigation of density fluctuations in high-speed jets and correlation with generated noise. J Fluid Mech 450:97–130

Pandey A, Gregory JW (2015) Dynamic response characteristics of polymer/ceramic pressure-sensitive paint. In: Proc. of: The 53rd Aerospace Sciences Meeting, AIAA-2015-0021

Pastuhoff M, Yorita D, Asai K, Alfredsson PH (2013) Enhancing the signal-noise ration of pressure-sensitive paint data by singular value decomposition. Meas Sci Technol 24:075301

Peng D, Wang S, Liu Y (2016) Fast PSP measurements of wall-pressure fluctuation in low-speed flows: improvements using proper orthogonal decomposition. Exp Fluids 57(4):45

Roozeboom NH, Diosady LT, Murman SM, Burnside NJ, Panda J, Ross JC (2016) Unsteady PSP measurements on a flat plate subject to vortex shedding from a rectangular prism. In: 54th AIAA Aerospace Sciences Meeting

Sakaue H, Kakisako T, Ishikawa H (2011) Characterization and optimization of polymer-ceramic pressure-sensitive paint by controlling polymer content. Sensors 11(7):6967–6977

Scroggin AM, Slamovich EB, Crafton JW, Lachendro N, Sullivan JP (1999) Porous polymer/ceramic composites for luminescent-based temperature and pressure measurement. MRS Proc 560:347. https://doi.org/10.1557/PROC-560-347

Sugimoto T, Kitashima S, Numata D, Nagai H, Asai K (2012) Characterization of frequency response of pressure-sensitive paints. In: Proc. of: The 50th AIAA Aerospace Sciences Meeting including the New Horizons Forum and Aerospace Exposition, AIAA-2012-1185

Sugioka Y, Numata D, Asai K, Koike S, Nakkita K, Nakajima T (2018) Polymer/ceramic pressure-sensitive paint with reduced roughness for unsteady measurement in transonic flow. AIAA J 56(6):2145–2156

Sugioka Y, Hiura K, Chen L, Matsui A, Morita K, Nonomura T, Asai K (2019) Unsteady pressure sensitive paint (PSP) measurement in low-speed flow: characteristic mode decomposition and noise floor analysis. Exp Fluids 60:108. https://doi.org/10.1007/s00348-019-2755-9

Yorita D, Numata D, Nagai H, Asai K (2010) Measuring unsteady low-speed flow phenomena by using a time-series analysis of pressure-sensitive paint images. In: Proc. 14th Int. Symp. on Flow Visualization. ISFV14-9E – 1